IEEE Photonics Journal
An IEEE Photonics Society Publication

Open Access

Dynamic Device Characteristics and Linewidth Measurement of InGaN/GaN Laser Diodes

Volume 13, Number 1, February 2021

Steffan Gwyn
Scott Watson
Thomas Slight
Martin Knapp
Shaun Viola
Pavlo Ivanov
Weikang Zhang
Amit Yadav
Edik Rafailov
Mohsin Haji
Kevin E Doherty
Szymon Stanczyk
Szymon Grzanka
Piotr Perlin
Stephen P Najda
Mike Leszczyski
Anthony E Kelly

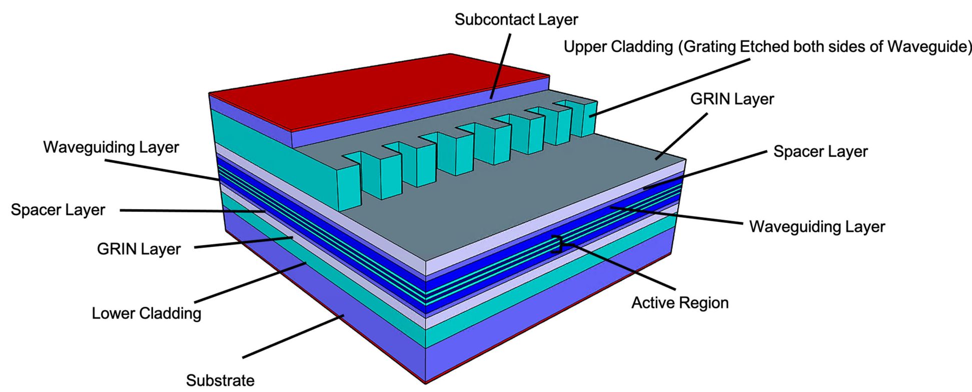

DOI: 10.1109/JPHOT.2020.3045218

Dynamic Device Characteristics and Linewidth Measurement of InGaN/GaN Laser Diodes

Steffan Gwyn,[1,2] **Scott Watson**,[1] **Thomas Slight**,[3] **Martin Knapp**,[4] **Shaun Viola**,[1] **Pavlo Ivanov**,[1,3] **Weikang Zhang**,[1] **Amit Yadav**,[5] **Edik Rafailov**,[5] **Mohsin Haji**,[4] **Kevin E Doherty**,[6] **Szymon Stanczyk**,[7] **Szymon Grzanka**,[7] **Piotr Perlin**,[7] **Stephen P Najda**,[7] **Mike Leszczyski**,[7] **and Anthony E Kelly**[1]

[1]School of Engineering, University of Glasgow, Glasgow G12 8LT, U.K.
[2]School of Mathematics and Physics, Queen's University Belfast, Belfast BT7 1NN, U.K.
[3]Compound Semiconductor Technologies Global Ltd., Glasgow G72 0BN, U.K.
[4]National Physical Laboratory, Teddington TW11 0LW, U.K.
[5]Aston University, Birmingham B4 7ET, U.K.
[6]Kelvin Nanotechnology, Glasgow G12 8LS, U.K.
[7]TopGaN Lasers, 01-142 Warsaw, Poland

DOI:10.1109/JPHOT.2020.3045218

Manuscript received November 20, 2020; revised December 4, 2020; accepted December 11, 2020. Date of publication December 16, 2020; date of current version December 31, 2020. This work was supported in part by the European Union under Grant E113162, in part by Innovate U.K. under Grant 132543, in part by the National Centre for Research and Development under Grant E113162/NCBiR/2020, and in part by the Engineering and Physical Sciences Research Council RCUK under Grant EP/L015323/1. *(Steffan Gwyn and Scott Watson have contributed equally to this work).*
Corresponding Author: Steffan Gwyn (e-mail: s.gwyn.1@research.gla.ac.uk).

Abstract: We report on the characterization and analysis of a GaN-based distributed feedback laser diode (DFB-LD) with 3rd-order laterally etched sidewall gratings centered at a wavelength of 420 nm. We also compare the device parameters with two commonly used Fabry-Perot (FP) devices operating at 450 nm and 520 nm. Intrinsic properties of the devices were extracted, including damping factor, carrier and photon lifetimes, modulation efficiency, differential gain, and parasitic capacitance. These parameters showed that the DFB exhibits a lower damping rate and parasitic capacitance while demonstrating a higher modulation efficiency, indicating that the DFB shows good potential for communications applications. Additionally, spectral linewidth of a GaN DFB is reported. To the authors' knowledge, this is the first demonstration of parameter extraction and spectral linewidth measurement for GaN-based DFB-LDs.

Index Terms: Gallium Nitride, distributed feedback laser diode, optical communications.

1. Introduction

Gallium Nitride (GaN)-based devices have been the focal point of significant research interest over the past three decades, since Nakamura demonstrated their value as LEDs [1]. In particular, GaN-based laser diodes (LDs) are a potentially key component in visible light communication (VLC) systems, with higher modulation bandwidth and output power capabilities compared to their LED counterparts. Standard Fabry-Perot (FP) GaN LDs have shown high bandwidths, allowing communication at data rates of multiple gigabits per second [2], [3]. However, for many applications, such as cold atom systems [4], spectroscopy [5], medical diagnostics [6], and underwater optical

communications [7], [8], spectral purity and the ability to select and tune specific wavelengths is extremely important [9]. To address this issue, the development of single-mode GaN-based LDs emitting at blue and green wavelengths have been recently reported [10]–[12]. One major issue observed in all GaN distributed feedback (DFB) LDs previously reported is the high threshold current, resulting in thermal degradation issues which can affect device reliability. Additionally, while the basic characteristics of these devices have been reported, the underlying mechanisms that dictate the behavior of GaN-based DFB LDs have not. This work investigates these device properties through frequency response subtraction analysis, implementing a method first proposed by Morton *et al.* [13]. By calculating parameters such as the resonance frequency and damping rate of a device, important properties ranging from carrier and photon lifetimes (T_c and T_p, respectively) to differential gain (*g'*) can be derived. From T_c and T_p, one can deduce how carriers and photons interact within the active region, and therefore provide an insight into the internal quantum efficiency (IQE) [14] of the device. Differential gain, on the other hand, is an important parameter in the derivation of modulation efficiency, which indicates the speeds at which an LD can communicate data, as well as spectral linewidth, understanding of which is vital for the previously mentioned applications [15]. A narrow spectral linewidth ensures that minimal chromatic dispersion occurs, and for quantum applications such as atomic clocks the linewidth frequency must be narrower than the atomic transition being targeted, ensuring that atoms can be cooled efficiently [16]. Whilst these parameters have been well established in InP [17]–[19] and GaAs [20]–[23] DFB lasers, this is not the case for GaN devices. GaN LEDs have been the subject of vigorous research in terms of their recombination coefficients [24]–[26], while modulation efficiency and differential gain have been reported only for GaN FPs [27], [28]. This work will better characterize the carrier transport effects found in GaN-based DFBs, and indicate where improvements need to occur such that visible light devices can compete with the modulation characteristics of more established telecommunications LD technologies. Additionally, the results found for the DFB device will be compared to calculated values for commercial blue and green GaN FP devices, to demonstrate the feasibility of GaN-based laterally-coupled (LC) DFBs for the applications previously mentioned. These devices have been well-investigated by several research groups [2], [27], [29]–[33], and thus provide a benchmark for GaN-based device performance. Through comparison of their extracted parameters, one can draw conclusions as to GaN DFB suitability for applications such as optical communications, where there have been notable research drives for GaN LD technologies.

Following investigation into parameter extraction methods for GaN DFBs, spectral linewidth measurements will be discussed. This is a particularly important parameter for quantum cooling applications, as well as in communications applications, where a narrow linewidth can allow for precise wavelength division multiplexed (WDM) systems. This setup would require several devices, with central wavelengths separated by as little as 1 nm, operating in a multiplexed system for high data rate VLC systems, similar to that described in [31], which is a potential application with suitable optical filtering [34].

2. Device Properties

2.1 DFB Device Structure

Fig. 1 shows the LC-DFB structure, with full fabrication details outlined in [35], [36]. A standard ridge waveguide laser diode was originally fabricated, with the following epi-layers, from top to bottom:

- GaN:Mg subcontact layer.
- AlGaN:Mg cladding layer.
- AlGaN:Mg graded index (GRIN) layer.
- GaN spacer layer.
- InGaN waveguiding layer.
- 2 x InGaN quantum wells, with GaN barriers.
- InGaN:Si waveguiding layer.

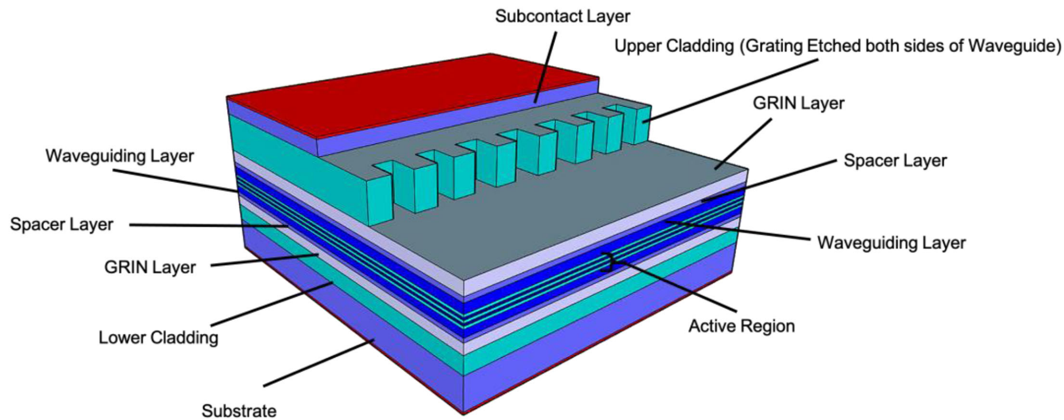

Fig. 1. Design of a typical GaN-based LC-DFB with a deeply-etched sidewall grating. Note: this diagram is not to scale.

- GaN:Si technical layer.
- AlGaN:Si GRIN layer.
- AlGaN cladding layer.

Gratings were then etched laterally into the sidewall of the ridge, down to the top of the upper waveguiding layer, at an etch depth of 580 nm, such that a GaN-based LC-DFB could be fully realized. This fabrication method was chosen because the complex overgrowth steps required to fabricate a buried heterostructure DFB are not currently possible in GaN [37], and surface gratings can damage the p-contact [38], resulting in increased losses in areas without electrical pumping. This is one of the more straightforward routes to single-wavelength emission, requiring only a minor modification of a standard ridge waveguide process. The main additional difficulty is the deep and vertical semiconductor etch to form the sidewall notches. 1st-order gratings would be challenging to fabricate at the intended wavelength, as feature sizes of $\sim$40 nm would be required for emission at $\sim$400 nm [33] with etch depths of $\sim$600 nm. Therefore, a 3rd-order grating was implemented, with feature sizes of $\sim$120 nm, and an 80% duty cycle to achieve coupling strengths comparable to that observed in a 1st-order grating [39]. The device used was a 3rd-order grating DFB without facet coatings, with a cavity length of 500 μm, and mounted p-side up in a TO5.6 package.

2.2 Device Characterization

Firstly, the LVI characteristics of the device were investigated at a constant temperature of 17 °C, and are shown in Fig. 2(a). The device has a threshold current of 32 mA at a threshold voltage of 8.2 V, and exhibits a differential series resistance of approximately 40 Ω. This high value is in part due to the reduced contact area associated with the LC-DFB design. A single-mode output power of 11 mW is achieved. Comparing the threshold current to previously reported devices [10]–[12], [35], [36], however, it is markedly lower than what has been observed before, through wavelength alignment of the gain peak and grating stopband. The reduced threshold current would result in fewer thermal degradation issues, and therefore improve device reliability and lifetime [40]. The emission spectra of the device were acquired using a high-resolution 1m-long spectrometer (FHR1000 Horiba Jobin Yvon), a Synapse 2048 x 512 CCD camera, and a 3600 groove-per-mm diffraction grating, shown in Fig. 2 (b). This setup provides a resolution of $\sim$6.2 pm for emission at a wavelength of 420 nm, which is an order of magnitude below the expected FP mode spacing in the GaN device. At 70 mA, mode-hopping behavior is evident, with multiple peaks observable and a wavelength hop to high wavelength. A wavelength hop of around 0.8 nm occurs, the cause of which is unlikely to be related to the DFB stopband, as this would yield a coupling coefficient of $\kappa \approx$ 350 cm^{-1} [41], which in comparison to the calculated values in [35] is too large. The jump is more

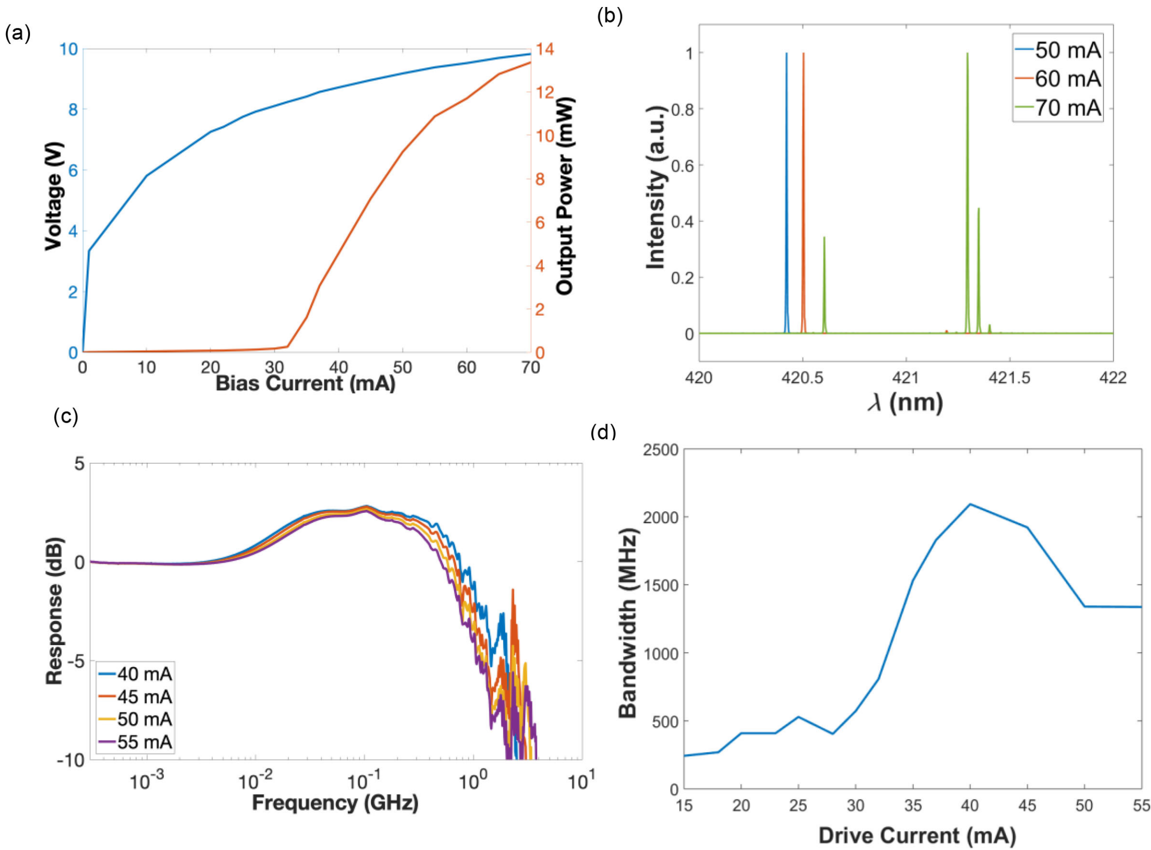

Fig. 2. (a) LVI characteristics of the GaN DFB with increasing bias current. (b) Spectral characteristics of the GaN DFB with increasing bias current. (c) Frequency Response of the GaN DFB at various bias currents. (d) Optical -3dB bandwidths with increasing bias current.

likely to arise from the emergence of the first-order transverse mode, since the calculated modal index changes between the zeroth-order and TE01 modes are consistent with this observed shift in the DFB stopband. This is also observed in Fig. 2 (a), with kinks visible between 60 and 70 mA. The tuning coefficient of the device with current was measured to be 0.015 nm/mA. In comparison, commercially available FP devices were found to have tuning coefficients of 0.03 nm/mA, and a reduced tuning coefficient indicates higher wavelength selectability, and therefore that the device tested is indeed a DFB.

3. Results and Analysis

3.1 Frequency Response

Following steady-state measurements, frequency response measurements were taken. The laser light was focused onto an ALPHALAS UPD-30-VSG-P Ultrafast photodetector, which has a bandwidth of 10 GHz. Using this setup, the optical −3 dB bandwidths were calculated at varying bias currents, and are shown in Fig. 2 (c). There is a rise in the response of the device after 100 MHz due to inductive peaking between the chip and package [42]. Fig. 2 (d) shows the bandwidth of the device plotted against bias current. The maximum bandwidth of 2.1 GHz occurs at 40 mA, and starts to decrease after this. As the bandwidth of the detector is 10 GHz, this is not a likely limiting factor. Parasitic capacitance within the device and package are the likeliest candidates for the limitations in this measured bandwidth.

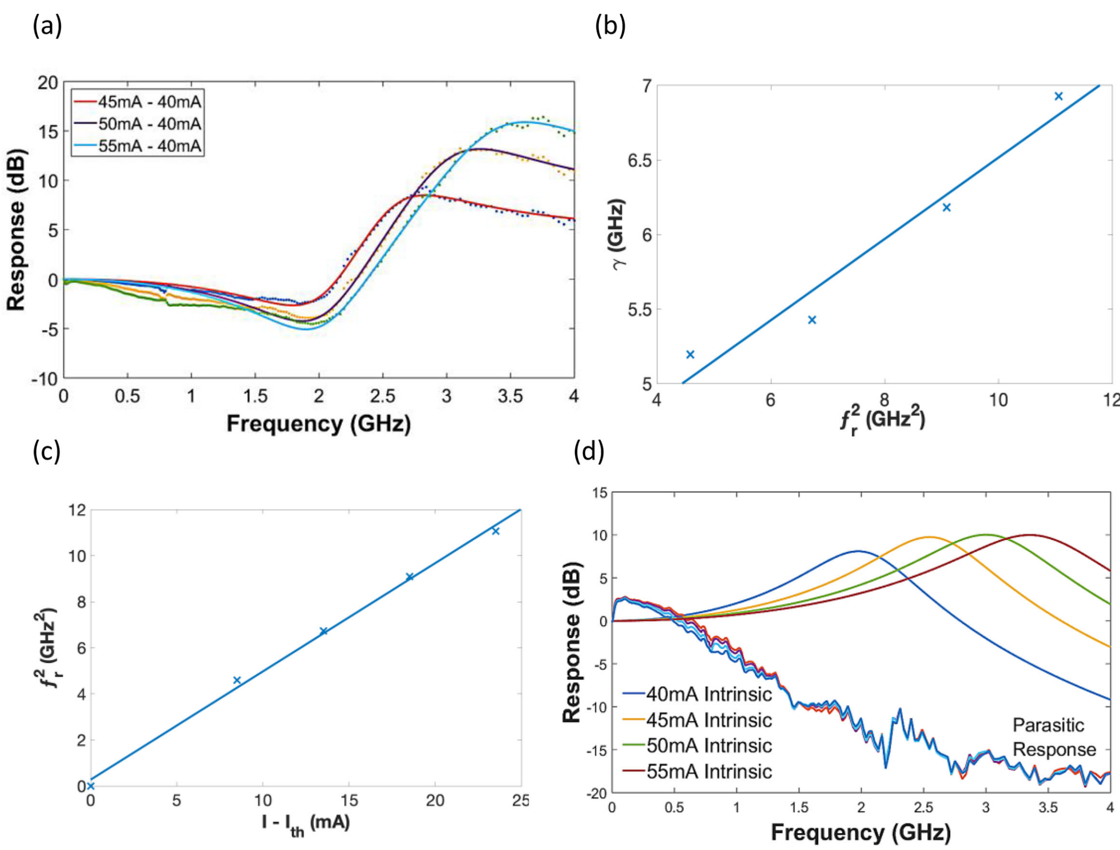

Fig. 3. (a) Subtracted frequency response at varying bias current. (b) Damping factor against the square of resonant frequency for the GaN DFB. (c) Plot of the square of resonant frequency against bias current above threshold for the GaN DFB. (d) Calculated intrinsic and parasitic response for the GaN DFB.

3.2 Parameter Extraction

To remove any effects caused by extrinsic factors such as parasitics, and subsequently acquire the dynamic device characteristics, parameter extraction was performed as per Morton *et al.* [13]. This has been used extensively in InP and GaAs devices, however to the author's knowledge has never been reported in GaN DFB lasers. To remove parasitic effects which remain constant with bias, the response at low bias current is subtracted from a higher bias and then fitted as in [13]. Typical fits are shown in Fig. 3 (a), with the frequency response at 40 mA being subtracted from that at 45 mA, 50 mA and 55 mA. From Fig. 3 (a), there is good agreement between the calculated fit and experimental data. The remaining response is then fitted to reveal the values of resonant frequency (f_r) and damping rate (γ) at each bias. The $|R|^2$ value was above 95% for each curve, indicating a good fit to the experimental data. The values found for f_r and γ are lower than those which are typical in AlGaAs or InP-based systems [43]. This arises from the dependency of resonant frequency on parameters such as differential gain and photon density above threshold [44]. γ is related to f_r by $\gamma = Kf_r^2 + {}^1/_{\tau_c}$ [45], where T_c is the effective carrier lifetime in the device, i.e., the sum of all carrier recombination methods. K is the damping factor of the DFB, which is directly related to the photon lifetime T_p as $K = 4\pi^2\tau_p$ [44]. Therefore, by plotting γ against $f_r{}^2$, one can find both the carrier and photon lifetimes for the GaN DFB. This is shown in Fig. 3 (b). Through calculating the gradient and intercept of the line, values of K = 0.23 ns (T_p = 5.83 ps), and T_c = 0.25 ns were found. These values are similar to that found for InP lasers [43], while the carrier lifetime found is an order of magnitude lower than that for previous work in the GaN material system [28]. This may be due to increased non-radiative recombination due to the larger surface area in

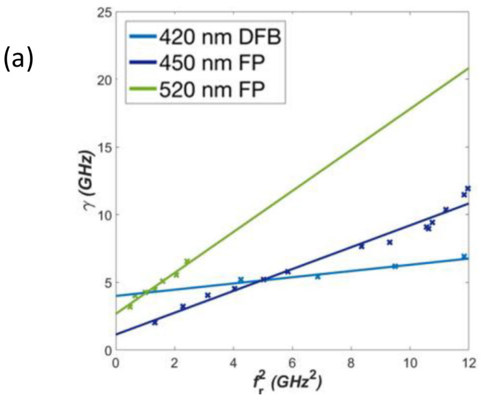

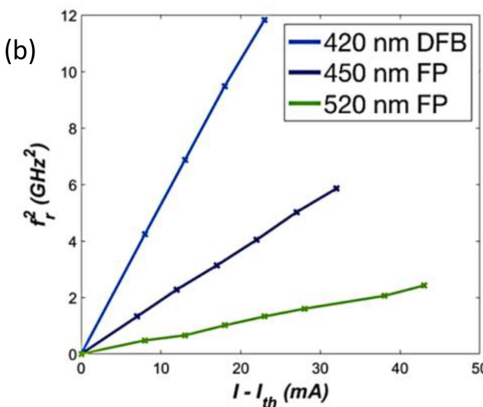

Fig. 4. (a) Comparison of Fig 3(b) for the GaN DFB against two commercial GaN FPs, one OSRAM PL450B and one ORSAM PL520B. (b) Comparison of Fig 4(a) for the same devices as in (a).

the grating. A relation can also be found between bias current and resonant frequency through the equation $f_r^2 = D(I - I_{th})$, where

$$D = \frac{\eta v_g \Gamma g'}{4\pi^2 Ve} \tag{1}$$

is the square of the modulation efficiency of the device [38]. Here, η is the IQE, v_g is the group velocity, Γ is the confinement factor, V is the active volume and e is the electron charge. Fig. 3 (c) shows the square of resonant frequency against current above threshold. Using the gradient of the line in Fig. 3 (c), it is found that D = 0.51 GHz^2/mA, corresponding to a modulation efficiency of 0.71 GHz/mA$^{0.5}$. From here, using known values for constants contained within D [40], as well as values calculated for v_g, Γ, and V through simulations using RSoft's LaserMOD software tool, a differential gain of $g' = 7.42 \times 10^{-16}$ cm^2 was estimated. For lasers in more well established materials such as InP and GaAs, D and g' are typically an order of magnitude higher [18], [22], [23], however in previous reported works for GaN FP devices, D was found to be significantly lower, ranging from ~0.1 GHz/mA$^{0.5}$ [27] to ~0.5 GHz/mA$^{0.5}$ [28]. Finally, from the values found for f_r and γ, the intrinsic response was found for the GaN DFB. The intrinsic response and subsequent parasitic response, which is equivalent to the calculated intrinsic response subtracted from the experimental results, is shown in Fig. 3 (d). The parasitic response remains constant with increasing bias. Using calculated values for series resistance of the device, the parasitic capacitance was found to be 7.7 pF. High speed operation (>10 GHz) requires the parasitic capacitance to be an order of magnitude lower [46], as well as a reduction in series resistance. The intrinsic 3 dB bandwidths increase with bias current, and intrinsic bandwidths up to 5.87 GHz were found for the device at 55 mA, suggesting 10 Gbit/s direct modulation may be possible.

3.3 Comparison With Commercial Devices

The previous experiments were also undertaken for one blue GaN FP device, an OSRAM PL450B centered at 450 nm, and one green GaN FP device, an OSRAM PL520B centered at 520 nm. These devices have been consistently researched for their properties, and as such are a notable benchmark to compare a GaN-based DFB to. Following parameter extraction, comparisons can be drawn between the DFB and commercial devices. Fig. 4(a) shows the plot used to calculate carrier and photon lifetimes as before in Fig. 3(b), but for the DFB and commercial FPs. From Fig. 4(a), the value of the damping rate K, and therefore the photon lifetime, is much smaller for the DFB compared to the FPs, with photon lifetimes of 20.4 ps and 38 ps for the blue and green FPs respectively, compared to 5.8 ps for the DFB. Additionally, the carrier lifetime calculated for the blue FP and green FP is 0.87 ns and 0.37 ns respectively, while the DFB exhibits a carrier lifetime of 0.25

TABLE 1
Comparison of Calculated Parameters Between the DFB, Blue FP, and Green FP

	420 nm DFB	450 nm FP	520 nm FP
τ_p (ps)	5.83	20.4	38
τ_c (ns)	0.25	0.87	0.37
D (GHz/mA$^{0.5}$)	0.71	0.42	0.24
Parasitic Capacitance (pF)	7.7	51.2	34.8
Series Resistance (Ω)	40	14	9

ns. For a LD to operate at high data rates, a low photon lifetime is desired, such that the damping rate is minimized and therefore the maximum 3 dB bandwidth is optimized [44]. This indicates that the DFB has more potential for data communication at high bit rates than commercial devices, which is promising especially in underwater communications, where visible light communications are of particular interest [8].

Fig. 4(b), on the other hand, indicates the modulation efficiency for the three devices, as in Fig.3(c). The calculated modulation efficiency for the commercial devices are 0.42 GHz/mA$^{0.5}$ and 0.24 GHz/mA$^{0.5}$ for the blue and green FPs respectively, both of which are markedly lower than the 0.71 GHz/mA$^{0.5}$ found for the GaN DFB. The parasitic capacitance of the devices were calculated to be 51.2 pF and 34.8 pF for the blue and green devices respectively, while the DFB chip exhibits a parasitic capacitance of 7.7 pF. Table 1 shows the values of carrier and photon lifetimes, modulation efficiency, and parasitic capacitance for each device. Overall these values allude to the LC-DFB device being extremely compatible with optical communications applications compared to its FP counterparts, with faster photon recombination, an increased modulation efficiency, and improved parasitic capacitance.

3.4 GaN DFB Linewidths

In addition to the parameters found through the subtraction method, the laser spectral linewidth is an important device characteristic in many applications for which GaN DFBs are desirable, including atomic cooling of Strontium ions ($^{88}Sr^{+}$) [47]. Current state-of-the-art quantum clocks require bulky tabletop laser systems [48], with extra apparatus required for frequency doubling to achieve the target cooling wavelength of 422 nm. A suitable laser diode, such as the one described here, would be an attractive alternative to realize a portable clock system. A narrow spectral linewidth is imperative, such that the laser can lock onto the transition accurately and robustly. The Schawlow-Townes formula outlines the parameters that control spectral linewidth [49]:

$$\Delta\nu = \Gamma \frac{r_{sp}}{R_{sp}} \frac{hf\,(\alpha_i + \alpha_m)\,\alpha_m (1 + \alpha_H)^2}{4\pi P_{out}} \tag{2}$$

From (2), low propagation and mirror losses (α_i and α_m respectively), a reduced confinement factor and linewidth enhancement factor (α_H), and increased output power lead to a narrow linewidth, as the photon energy (hf) and spontaneous emission factor (r_{sp}/R_{sp}) remain constant.

To acquire the laser linewidth, a scanning Fabry-Pérot interferometer was utilized [50], with a resolution accuracy of 6 MHz. The light from the DFB laser was collected using a collimating lens and was aligned onto the interferometer. The light was directed using mirrors and the associated software was used to ensure the spot size was correct and that the full beam was focused at the input. A linewidth of 18.7 MHz was acquired for a similar device to what was used for parameter extraction, as shown in Fig. 5 (a). Fig. 5 (b) shows the expected relationship of linewidth as a function of inverse power.

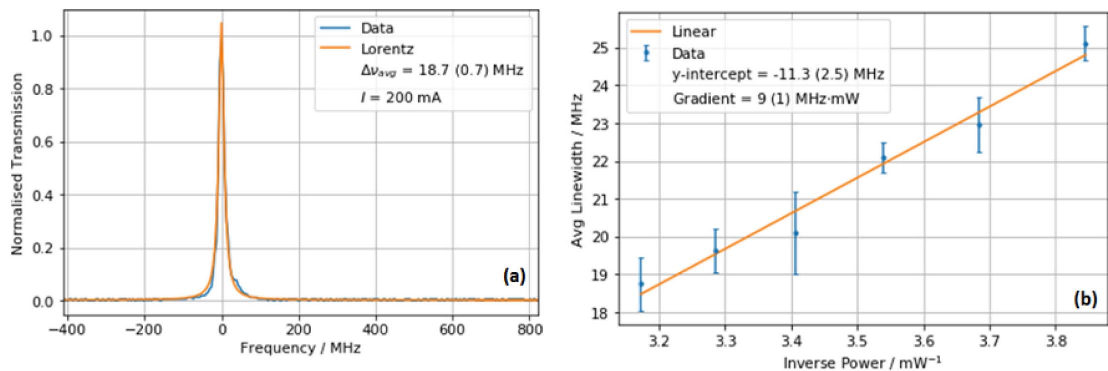

Fig. 5. (a) GaN DFB Laser linewidth using scanning Fabry-Pérot interferometry, with system uncertainties highlighted in brackets. (b) Relation of linewidth with inverse optical power for the GaN DFB.

Typically, linewidth of the order of $\sim$1 MHz are required for atomic cooling applications. As GaN DFBs are a relatively new technology, these spectral linewidths are currently being optimized in order to fully realize their suitability for quantum applications.

3.5 Improvements to GaN DFBs

To improve the high-speed modulation capabilities, the differential gain needs to be increased, and device length should be reduced. Differential gain improvements could be achieved by improvement in material quality and increasing the number of wells and hence confinement factor. Reduced length whilst maintaining DFB operation requires an increase in coupling coefficient κ, which is difficult to achieve in LC-DFBs. Changing the grating width [26] or depth to increase κ is possible in this case, but the upper value of coupling coefficient is limited by the maximum achievable index change via this grating geometry. A buried grating would be desirable, but as previously mentioned the overgrowth steps required are not feasible in GaN. Further improvements may require epitaxial design changes.

In terms of spectral linewidth, atomic cooling applications require $<$1 MHz linewidth [4] which requires significant improvements over current performance. These could be achieved through the application of dielectric facet coatings, reduction of cavity loss, the use of grating phase shifts, and the general improvement of laser performance to increase output power. Ideally, the range at which the device works in single mode operation will be increased, allowing measurements at higher powers and ultimately resulting in lower linewidths.

4. Conclusion

In this work, intrinsic parameters of GaN laser diodes were ascertained for the first time. Three GaN-based LDs, one DFB and two commercial FPs, were characterized, and the intrinsic response of the devices were determined. The damping factor, carrier and photon lifetime, modulation efficiency, differential gain and parasitic capacitance were all calculated, with improved performance shown by the DFB compared to the FPs. The results were also comparable to those found in more well-established telecommunications lasers. This indicates the possibility of high-speed direct modulation of single-frequency blue lasers.

Acknowledgement

The authors would like to thank Dr Guilong Huang for their assistance in the experimental setup for linewidth measurement.

References

[1] S. Nakamura, T. Mukai, and M. Senoh, "Candela-class high-brightness InGaN/AlGaN double-heterostructure blue-light-emitting diodes," *Appl. Phys. Lett.*, vol. 64, pp. 1687–1689, 1994.

[2] S. Watson *et al.*, "Visible light communications using a directly modulated 422 nm GaN laser diode," *Opt. Lett.*, vol. 38, pp. 3792–3794, 2013.

[3] W. S. Tai, H. H. Lu, H. W. Wu, C. W. Su, and Y. C. Huang, "A 30 Gb/s PAM4 underwater wireless laser transmission system with optical beam reducer/expander," *Sci. Rep.*, vol. 9, 2019, Art. no. 8605.

[4] A. Shiner, "Development of a frequency stabilized 422-nm diode laser system and its application to a $^{88}Sr^{+}$single ion optical frequency standard," MSc Thesis, Dept. Faculty Graduate Sci., York University, Toronto, 2006.

[5] B. Li *et al.*, "Sensitive Raman gas analysis using a 500mW external cavity diode laser at 410 nm," *Laser Phys. Lett.*, vol. 14, 2017, Art. no. 095701.

[6] S. P. Najda *et al.*, "A multi-wavelength (u.v. to visible) laser system for early detection of oral cancer," in *Imag., Manipulation, Anal. Biomolecules, Cells Tissues XIII: Proc. SPIE Photon. West*, San Fransisco, USA, Sep.-Nov. Feb. 2015, ed., D. L. Farkas, D. V. Nicolau, and R. C. Leif, SPIE, Bellingham, USA, 2015, pp. 50–55.

[7] T. C. Wu, Y. C. Chi, H. Y. Wang, C. T. Tsai, and G. R. Lin, "Blue laser diode enables underwater communication at 12.4 Gbps," *Sci. Rep.*, vol. 7, 2017, Art. no. 408040.

[8] G. Giuliano, L. Laycock, D. Rowe, and A. E. Kelly, "Solar rejection in laser based optical communication systems," *Opt. Exp.*, vol. 25, 2017, Art. no. 33066.

[9] Y. Shimada *et al.*, "A simplified 461-nm laser system using blue laser diodes and a hollow cathode lamp for laser cooling of Sr," *Rev. Sci. Instrum.*, vol. 84, 2013, Art. no. 063101.

[10] H. Zhang *et al.*, "Continuous-wave operation of a semipolar InGaN distributed-feedback blue laser diode with a first-order indium tin oxide surface grating," *Opt. Lett.*, vol. 44, 2019, Art. no. 3106.

[11] J. A. Holguín-Lerma, T. K. Ng, and B. S. Ooi, "Narrow-line InGaN/GaN green laser diode with high-order distributed-feedback surface grating," *Appl. Phys. Exp.*, vol. 12, 2019.

[12] J. H. Kang *et al.*, "DFB laser diodes based on GaN using 10th order laterally coupled surface gratings," *IEEE Photon. Technol. Lett.*, vol. 30, pp. 231, 2018.

[13] P. Morton, T. Tanbun-Ek, R. Logan, A. Sergent, P. Sciortino, and D. Coblentz, "Frequency response subtraction for simple measurement of intrinsic laser dynamic properties," *IEEE Photon. Technol. Lett.*, vol. 4, pp. 133–136, 1992.

[14] S. Karpov, "ABC-model for interpretation of internal quantum efficiency and its droop in III-Nitride LEDs: A review," *Opt. Quantum Electron.*, vol. 47. pp. 1293–1303, 2015.

[15] Y. Arakawa and A. Yariv, "Theory of gain, modulation response, and spectral linewidth in AlGaAs quantum well lasers," *IEEE J. Quantum Electron.*, vol. 21, pp. 1666–1674, 1985.

[16] W. D. Phillips, "Nobel Lecture: Laser cooling and trapping of neutral atoms," *Rev. Mod. Phys.*, vol. 70, p. 721, 1998.

[17] H. Lipsanen, D. L. Coblentz, R. A. Logan, R. D. Yadvish, P. A. Morton, and H. Temkin, "High-speed InGaAs/InP multiple-quantum-well laser," *IEEE Photon. Technol. Lett.*, vol. 4, p. 673, 1992.

[18] O. K. Kwon, C. W. Lee, Y. A. Leem, K. S. Kim, S. H. Oh, and E. S. Nam, "1.5-μm and 10-Gbs^{-1} etched mesa buried heterostructure DFB-LD for datacenter networks," *Semicond. Sci. Technol.*, vol. 30, 2015, Art. no. 105010.

[19] T. Sadeev, D. Arsenijevic, and D. Bimberg, "Comparison of dynamic properties of InP/InAs quantum-dot and quantum-dash lasers," *Appl. Phys. Lett.*, vol. 109, 2016, Art. no. 161104.

[20] L. Bjerkan, A. Royset, L. Hafskjaer, and D. Myhre, "Measurement of laser parameters for simulation of high-speed fiberoptic systems," *J. Lightw. Technol.*, vol. 14, p. 839, 1996.

[21] R. Nagarajan, T. Fukushima, S. W. Corzine, and J. E. Bowers, "Effects of carrier transport on high-speed quantum well lasers," *Appl. Phys. Lett.*, vol. 59, 1991, Art. no. 1835.

[22] H. Cantú, A. McKee, D. Childs, S. Watson, and A. E. Kelly, "Dynamic performance of detuned ridge waveguide AlInGaAs distributed feedback laser diodes," *Microw. Opt. Technol. Lett.*, vol. 59, 2017, Art. no. 1468.

[23] J. D. Ralston *et al.*, "Control of differential gain, nonlinear gain and damping factor for high-speed application of GaAs-based MQW lasers.," *IEEE J. Quantum Electron.*, vol. 29, 1993, Art. no. 1648.

[24] R. P. Green, J. J. D. McKendry, D. Massoubre, E. D. Gu, M. D. Dawson, and A. E. Kelly, "Modulation bandwidth studies of recombination processes in blue and green InGaN quantum well micro-light-emitting diodes," *Appl. Phys. Lett*, vol. 102, 2013, Art. no. 091103.

[25] T. Lin, H. C. Kuo, X. D. Jiang, and Z. C. Feng, "Recombination pathways in green InGaN/GaN multiple quantum wells," *Nanoscale Res. Lett.*, vol. 12, p. 137, 2017.

[26] S. Lin, H. Cao, J. Li, X. Sun, H. Xiu, and L. Zhao, "Modulation and optoelectronic properties of GaN-based light-emitting diodes on GaN template," *Appl. Phys. Exp.*, vol. 11, 2018, Art. no. 122101.

[27] C. Lee *et al.*, "4 Gbps direct modulation of 450 nm GaN laser for high-speed visible light communication," *Opt. Exp.*, vol. 23, 2015, Art. no. 16232.

[28] W. G. Scheibenzuber, U. T. Schwarz, L. Sulmoni, J. Dorsaz, J.-F. Carlin, and N. Grandjean, "Recombination coefficients of GaN-based laser diodes," *J. Appl. Phys.*, vol. 109, 2011, Art. no. 093106.

[29] G. Li, F. Hu, P. Zou, C. Wang, G. R. Lin, and N. Chi, "Beyond 10 Gbps 450-nm GaN laser diode based visible light communication system utilizing probabilistic shaping bit loading scheme," in *Proc. 12th Int. Symp. Commun. Syst., Netw. Digit. Signal Process.*, 2020, pp. 1–4.

[30] H. M. Oubei *et al.*, "Wireless optical transmission of 450 nm, 3.2 Gbit/s 16-QAM-OFDM signals over 6.6 m underwater channel," in *Proc. Conf. Lasers Electro-Opt.*, 2016, Paper SW1F.1.

[31] H. Chun, A. Gomez, C. Quintana, W. Zhang, G. Faulkner, and D. O'Brien, "A wide-area coverage 35Gb/s visible light communications link for indoor wireless applications," *Sci. Rep.*, vol. 9, 2019, Art. no. 4952.

[32] D. Tsonev, S. Videv, and H. Haas, "Towards a 100 Gb/s visible light wireless access network," *Opt. Exp.*, vol. 23, 2019, Art. no. 1627.

[33] G. He, Z. Lv, C. Qiu, and Z. Liu, "Performance evaluation of 520 nm laser diode underwater wireless optical communication systems in the presence of oceanic turbulence," *SID Symp. Dig. Tech. Papers*, vol. 51, pp. 47–50, 2020.

[34] S. Gwyn *et al.*, "GaN-based distributed feedback laser diodes for optical communications," in *Proc. 4th Int. Conf. Appl. Opt. Photon.*, 2019, Art. no. 112070O.

[35] T. J. Slight, O. Odedina, W. Meredith, K. E. Docherty, and A. E. Kelly, "InGaN/GaN distributed feedback laser diodes with deeply etched sidewall gratings," *IEEE Photon. Technol. Lett.*, vol. 28, pp. 2886–2888, 2016.

[36] T. J. Slight *et al.*, "Continuous-wave operation of (Al,In)GaN distributed-feedback laser diodes high high-order notched gratings," *Appl. Phys. Exp.*, vol. 11, 2018.

[37] D. Hofstetter, R. L. Thornton, L. T. Romano, D. P. Bour, M. Kneissl, and R. M. Donaldson, "Room-temperature pulsed operation of an electrically injected InGaN/GaN multi-quantum well distributed feedback laser," *Appl. Phys. Lett.*, vol. 73, 1998, Art. no. 2158.

[38] S. J. Pearton, J. W. Lee, J. D. MacKenzie, C. R. Abernathy, and R. J. Shul, "Dry etch damage in InN, InGaN, and InAlN," *Appl. Phys. Lett.*, vol. 67, 1995, Art. no. 2329.

[39] D. Pierścińska *et al.*, "Examination of thermal properties and degradation of InGaN-based diode lasers by thermore-flectance spectroscopy and focused ion beam etching," *AIP Adv.*, vol. 7, 2017, Art. no. 075107.

[40] Y. L. Cao *et al.*, "Hybrid III-V/silicon laser with laterally coupled Bragg grating," *Opt. Exp.*, vol. 23, pp. 8800–8808, 2015.

[41] K. Kihara, H. Soda, H. Ishikawa, and H. Imai, "Evaluation of the coupling coefficient of a distributed feedback laser with residual facet reflectivity," *J. Appl. Phys.*, vol. 62, pp. 1526–1527, 1987.

[42] J. P. Babić, A. R. Totović, J. V. Crnjanski, M. M. Krstić, M. L. Mašanović, and D. M. Gvozdić, "Enhancement of the MQW-RSOA.s small signal modulation bandwidth by inductive peaking," *J. Lightw. Technol.*, vol. 37, pp. 1981–1989, 2019.

[43] I. Tomkos, I. Roudas, R. Hesse, N. Antoniades, A. Boskovic, and R. Vodhanel, "Extraction of laser rate equations parameters for representative simulation of metropolitan-area transmission systems and networks," *Opt. Comm.*, vol. 194, pp. 109–129, 2001.

[44] A. J. Millard, "High-speed modulation of semiconductor lasers and properties of silver-coated quantum-dot lasers," M.Sc. Thesis, Dept. Elect. Comput. Eng., University of Illinois at Urbana-Champaign, Urbana, 2010.

[45] C. Reese, E. Yablonovitch, S. Keller, B. Keller, and S. DenBaars, "Absolute internal quantum efficiency of an InGaN/GaN quantum well," in *Proc. Conf. Lasers Electro.-Opt.*, Anaheim, CA, USA, 1996, p. 472.

[46] H. I. Cantú, A. McKee, I. Eddie, and A. E. Kelly, "Frequency selectivity in directly modulated distributed feedback laser transmission operation using and impedance match tuning network," *IEEE J. Quantum Electron.*, vol. 50, pp. 106–111, 2014.

[47] S. Watson *et al.*, "Distributed feedback lasers for quantum cooling applications," in *Proc. 22nd Int. Conf. Transparent Opt. Netw.*, 2020, pp. 1–4.

[48] A. D. Ludlow, M. M. Boyd, J. Ye, E. Peik, and P. O. Schmidt, "Optical atomic clocks," *Rev. Mod. Phys.*, vol. 87, pp. 637–701, 2015.

[49] C. Henry, "Theory of the phase noise and power spectrum of a single mode injection laser," *IEEE J. Quantum Electron.*, vol. 19, pp. 1391–1397, 1983.

[50] T. Takakura, K. Iga, and T. Tako, "Linewidth measurement of a single longitudinal mode AlGaAs laser with a Fabry-Perot interferometer," *Jpn. J. Appl. Phys.*, vol. 19, 1980, Paper L725.